Production of ice slurry in a scraped-surface plate heat exchanger

D. S. Martínez, J. P. Solano, F. Illán, A. Viedma

Universidad Politécnica de Cartagena, Departamento de Ingeniería Térmica y de Fluidos, C/Doctor Fleming s/n, Campus Muralla del Mar, 30202 Cartagena (Spain)

E-mail: davids.martinez@upct.es

Abstract.

The present work presents experimental results of the production of ice slurry in an innovative scraped-surface plate heat exchanger (SSPHE). It consists of a 28 liters capacity tank with a total heat transfer area of $10 m^2 m^{-3}$ crystallizer volume. The scraper consists of four rotating PEEK blades that are driven by a vertical shaft connected to an electrical motor. The heat transfer surface is cooled underneath by a flow of calcium chloride solution in water. The coolant solution is subsequently cooled by the expansion of a flow of R507 refrigerant in a compact evaporator. Sodium chloride brine with a concentration of 5% is the base solution for the generation of ice slurries of about 20% of ice content in a batch process.

1. Introduction

Ice slurries consist of aqueous solutions in which small ice crystals are present. One of the main advantages of ice slurries compared with the storage and usage of common ice is the easiest transport capacity, being possible to pump it. Clearly, the use as refrigerant offers the major benefit of ice slurries, owing to their high cooling capacity and constant cooling temperature.

Ice slurries are generally obtained from electrolytic solutions with a freezing point lower than the pure water one. There are a number of methods available for the production of these small ice crystals. Among them, the use of scraped surface heat exchangers (SSHE) is benefited by the high heat transfer coefficients induced in the process. The continuous scraping interrupts the boundary layer formation and moreover enhances the heat transfer between the wall and its surroundings [1]. On the other hand, the continuous scraping prevents the ice crystals growth in the heat transfer surface above a limited size.

Several investigations have been reported in the open literature on the production of ice slurries with Votator-type SSHE, where an inner cylindrical surface is continuously scraped by means of rotating blades. Qin et al [3] described the three stages in which the formation of the ice slurry occurs: chilling, nucleation and crystallization. The same authors reported afterwards a study on the heat transfer and power consumption in a SSHE while freezing aqueous solutions. However, they did not measure the temperatures at the heat transfer wall. The effect of the electrolyte concentration and the scraping velocity have been studied by Vaessen et al [2], who compared two types of scraped surface heat exchangers (cooled column disc and scraper cooled wall), finding that for both designs the transport of heat from process liquid to cooled wall surfaces at various rotational speeds of the scrapers can be accurately described by the

penetration theory. They also observed that the increase of the ice content of the crystallizer probably dominates over the increase of the scraping speed. The process-side heat transfer therefore decreases at higher temperature differences and scraping rates. In spite of the wide work presented, the heat transfer coefficients were indirectly obtained from the ice slurry and coolant temperatures, but they did not consider the temperature of the scraped wall. Different experimental techniques like Particle Image Velocimetry (to study the flow pattern) and liquid crystal thermometry (to study heat transfer) have been applied also to scraped surface plate heat exchangers employed in the production of ice slurries [4].

In light of the previous studies, the aim of this work is to experimentally investigate the heat transfer process involved in the ice slurry production using an innovative scraped-surface plate heat exchanger (SSPHE). Transient experiments have been performed in order to assess the influence of the scraping rotational speed and power consumption in the production capacity, together with the coolant mass flow. Heat transfer coefficients have been calculated by measuring the freezing wall temperature and the ice slurry temperature. We report the process-side heat transfer enhancement induced in the freezing wall by the scraping effect of the rotating blades.

2. Ice slurry fundamentals

The required mass flow to achieve a certain cooling rate in a system with a unique liquid phase is given by,

$$\dot{Q} = \dot{m} c_p \Delta T = \dot{V} \rho c_p \Delta T \tag{1}$$

whereas in a system operating with ice slurry the above expression becomes,

$$\dot{Q} = \dot{m} \Delta h = \dot{V} \rho \Delta h \tag{2}$$

where $\dot{m}$ corresponds to the mass flow, $\dot{V}$ to the volumetric flow, ΔT is the inlet-outlet temperature change, ρ is the density and c_p is the specific heat. The enthalpy difference Δh includes both the sensible heat and the latent heat of fusion. The heat transport ability of the ice slurry in equilibrium is thus proportional to the enthalpy change Δh, which will always be much higher for the ice slurry than for a single phase water solution. Ice slurry production can be then described as

$$\dot{Q} = \frac{\dot{V}}{100} \left(c_h L_h + (100 - c_h) \rho c_p \right) \Big|_{t_1}^{t_2} \tag{3}$$

where now $\dot{Q}$ is the heat absorbed by the ice slurry between the time instants t_1 and t_2, c_h is the ice content (%) and L_h is the latent heat of fusion. The different thermophysical properties are evaluated at the brine temperature T_f. The heat $\dot{Q}$ is absorbed through the heat transfer surface, which is continuously scraped by the action of the blades. Starting from an initial electrolyte concentration, the increasing amount of ice in the solution (which only contains pure water) will lead to an increment of the electrolyte concentration in the remaining solution, decreasing in that way its freezing point. If the heat transfer surface is in turn cooled by a coolant brine, then it is possible to write that,

$$\dot{Q} = \dot{m}_c c_{p,c} \Delta T_c \tag{4}$$

where now $\dot{m}_c$ is the mass flow rate of coolant brine, $c_{p,c}$ is its specific heat and ΔT_C corresponds to the temperature difference between inlet and outlet.

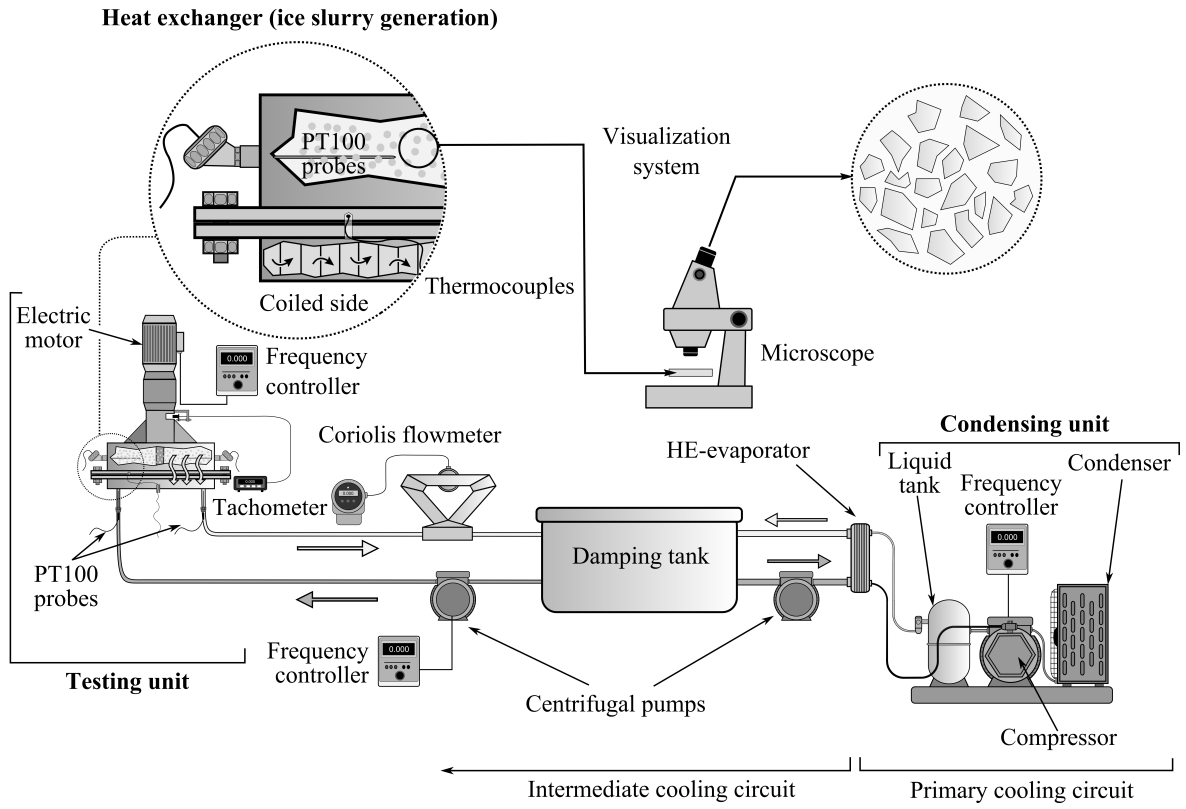

Figure 1. Schematic diagram of the experimental apparatus

3. Experimental set up and procedure

3.1. Experimental facility

A schematic diagram of the experimental set-up is presented in Fig. 1. The heat exchanger (ice slurry production unit) consists of a 28 liters AISI 316 tank of 600 mm diameter and 100 mm height with a scraped heat transfer surface at the bottom (see Fig. 2) of $10 m^2 m^{-3}$ crystallizer volume. The scraper consists of four rotating PEEK blades that are driven by a vertical shaft connected to an electrical motor. The heat transfer surface is cooled underneath by a flow of calcium chloride solution in water which flows across a coiled circuit. The coolant solution is subsequently cooled by the expansion of a flow of R507 refrigerant in a compact evaporator. A damping tank of 300 liters is used to avoid instabilities in the coolant temperature. Scraper velocity, coolant flow rate and compressor operating regime are all of them accurately settled by frequency controllers.

Regularly distributed thermocouples are embedded in the rear side of the heat transfer plate (see Fig. 2). They provide an indirect measurement of the wall temperature in the scraped surface while four immersed PT-100 sensors placed 90° apart circumferentially at 50 mm of height retrieve the bulk fluid temperature in the heat exchanger. The heat transfer to the cooling circuit is accounted for with PT-100 sensors which measure the inlet and outlet temperature of the coolant flow, whereas a Coriolis flow meter is used for obtaining the mass flow rate of coolant.

A sodium chloride brine with concentrations of 5% wt is employed in the SSPHE as the base solution for the generation of ice slurries in a batch process: the base solution is introduced in the SSPHE and it is continuously cooled by the calcium chloride flow until a certain percentage of

ice is reached (in this study 20%). The percentage of ice is determined from the ice slurry mean temperature (see Sec. 3.2) by using the available correlations in [5], as well as the thermophysical properties for the NaCl and $CaCl_2$ brines. The coolant temperature is kept constant during the test duration by means of a PID controller which regulates the frequency of the condensing unit compressor. Coolant temperature values are set in order to have a certain temperature difference $\Delta T_C = \overline{T}_{f,fp} - \overline{T}_c$ where $\overline{T}_{f,fp}$ is the predicted freezing point temperature ([5]) for the NaCl initial concentration in the test. Maximum differences of 0.2 °C were found between the expected and the obtained freezing point temperature.

The heat exchanger and the coolant tubes were insulated by an elastomeric thermal insulation material of 30 mm thickness and thermal conductivity 0.04 W/(m·K), in order to minimize heat losses to the ambient.

3.2. Calculation procedure

A schematic view of the heat exchanger working mechanism is depicted in Fig. 2. The stainless steel blade is inserted in the PEEK scraper material with an elastic rod between them, in order to absorb vertical efforts forces. A gap of $\delta \approx 0.7$ mm exists between the scraper and the 8 mm thick wall, where the thermocouples are embedded. The mean fluid temperature $\overline{T}_f$ is obtained by averaging the four immersed PT100 sensors, whereas the wall temperature $\overline{T}_w$ is obtained by averaging temperature values retrieved by the thermocouples. The inlet and outlet coolant temperatures (T_{ci} and T_{co} respectively) are averaged to obtain the mean coolant temperature $\overline{T}_c$.

The convective heat flux between the ice slurry and the heat transfer wall can be then quantitatively characterized by means of the heat transfer coefficient h, given by

$$h = \frac{\dot{Q}}{A\left(\overline{T}_f - \overline{T}_w\right)} \tag{5}$$

where A is the area of the heat transfer surface and $\overline{T}_w$ is its averaged temperature. The heat flux per unit area $q" = \dot{Q}/A$ is obtained from the Eq. 4, that now becomes,

$$\dot{Q} = \dot{m}_c c_p\Big|_{\overline{T}_c} (T_{co} - T_{ci}) \tag{6}$$

4. Results

Figure 4 shows the temporal evolution of the ice slurry temperature for a c_h =20% test. The initial part, before the starting of the nucleation, corresponds to the brine chilling. The brine temperature decreases until it underpasses the freezing point ($T_{fp} \approx -3.1$°C for 5% NaCl), entering in a state of non thermodynamical equilibrium. Then the temperature rises abruptly and the product becomes suddenly opaque due to the appearance of nucleation. The sensible heat accumulated during the supercooling is then transformed into latent heat by the formation of a multitude of ice crystals. The supercooling phenomenon has been used as an indicator of the size distribution of ice crystals, since it is greatly determined by the behaviour of ice nucleation and crystallization. This approach, known as the thermal response method, was proposed by Kane [6] and was further modified ([7], [8] and [9] among others). According to it the growing rate is proportional to the instantaneous supercooling. Several models exist to obtain the nucleation and crystallization parameters from the thermal response curve [11]. However, very high-resolution thermal probes are required to apply them and it escapes from the scope of the present work. Figure 3 shows a different temperature evolution where supercooling is not present and the nucleation starts without abrupt changes in the temperature. This different behaviour is related with the thermal stratification in the heat exchanger, as it is shown later. In

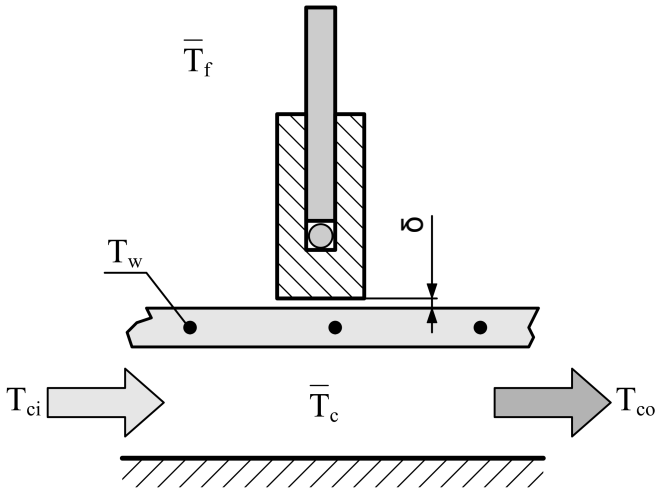

Figure 2. Cross sectional profile of the ice scraping system in the SSPHE

both cases the wall temperature is slightly above the coolant one, with a big difference between the wall and the fluid temperature. On the other hand, the change between the inlet and outlet coolant temperatures is always less than 0.5 °C, ensuring a uniform temperature along the coiled side of the heat exchanger.

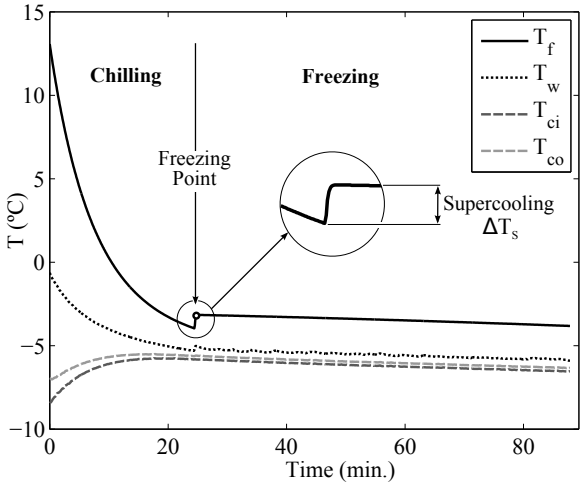

Figure 3. Averaged NaCl brine-ice slurry temperature ($\overline{T}_f$), averaged wall temperature ($\overline{T}_w$) and coolant inlet and outlet temperatures (T_{ci} and T_{co}) evolution with time during a common test (supercooling detected).

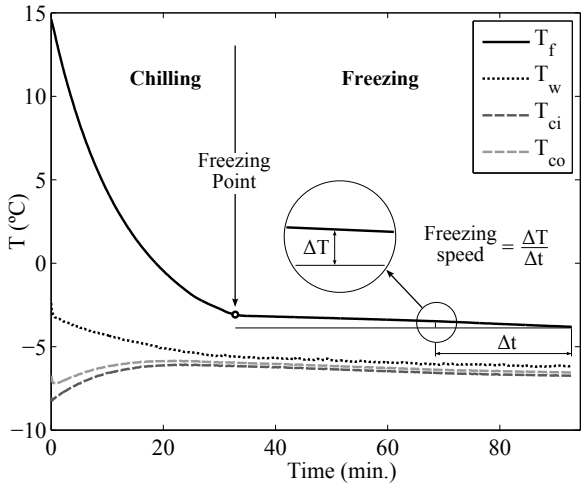

Figure 4. Averaged NaCl brine-ice slurry temperature ($\overline{T}_f$), averaged wall temperature ($\overline{T}_w$) and coolant inlet and outlet temperatures ($\overline{T}_{ci}$ and $\overline{T}_{co}$) evolution with time during a common test (no supercooling detected).

From the temperature evolution curve it is possible to define the freezing speed parameter ζ as the slope of the curve for instantaneous temperature evolution $\Delta T/\Delta t$. If the freezing process is divided into n successive time instants Δt_i starting at the beginning of the nucleation, an average freezing speed $\overline{\zeta}$ can be obtained as,

$$\overline{\zeta} = \frac{1}{n}\sum_{i=1}^{i=n}\frac{\Delta T_i}{\Delta t_i} \tag{7}$$

where ΔT_i is the temperature change for each time interval. The average freezing speed $\overline{\zeta}$ is then proportional to the ice slurry production rate. Figure 5 depicts the averaged freezing speed $\overline{\zeta}$ versus the averaged difference of temperatures ΔT_C along all the ice formation period $\overline{\Delta T}_C = \overline{\overline{T}_{f,fp} - \overline{T}_c}$. The color of each point corresponds to the rotating speed of the scrapers. It is clear from the figure that $\overline{\zeta}$ increases almost linearly until $\overline{\Delta T}_C \approx 3.5$ °C with a ratio of $\approx 1.1{\cdot}10^{-2}$ min^{-1}. After that point the ratio decreases until $\approx 10^{-3}$ min^{-1}. It is also possible to notice that the rotating speed of the scrapers has a poor influence in $\overline{\zeta}$.

The points where supercooling was not detected (square shape) corresponds to the lowest $\overline{\zeta}$ for each $\overline{\Delta T}_C$ value. Moreover, these points present always the lowest velocities and they appear after $\overline{\Delta T}_C$ reaches a minimum value. The presence or not of the supercooling phenomena indicates if the nucleation started at the same time in the whole the fluid volume. Due to the configuration of the heat exchanger, with the freezing wall in the bottom, the thermal stratification phenomenon is reinforced. In that scenario low scraping velocities and large values of $\overline{\Delta T}_C$ will lead to a stratified medium, where the nucleation can start in the bottom and rise then gradually. Therefore the temperature probes in the heat exchanger, placed at a height of $H/2$ will not detect the supercooling. The value of the supercooling amplitude ΔT_S is then not only related to the growing rate, but also to the thermal stratification in the volume. To elucidate this phenomenon the Richardson number (Ri), which evaluates the importance of natural convection relative to the forced convection, was calculated as,

$$Ri = \frac{g\beta\left(\overline{T}_f - \overline{T}_w\right)\frac{H}{2}}{\omega^2\frac{D^2}{4}} \tag{8}$$

where β (K^{-1}) is the thermal expansion coefficient [10], g is the gravitational acceleration and ω is the rotating velocity of the blades in rad·s^{-1}. Figure 6 shows the values of ΔT_S for the obtained Ri values at each $\overline{\Delta T}_C$, and coloured by the rotating velocity of the blades. $\overline{T}_f$ and $\overline{T}_w$ are evaluated at the supercooling instant (minimum $\overline{T}_f$) or at the nucleation starting point in the case of no supercooling detected.

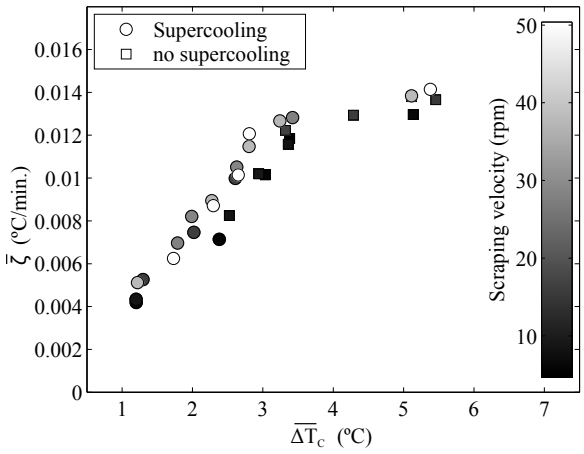

Figure 5. Averaged freezing speed $\overline{\zeta}$ vs. coolant temperature difference $\overline{\Delta T}_C$.

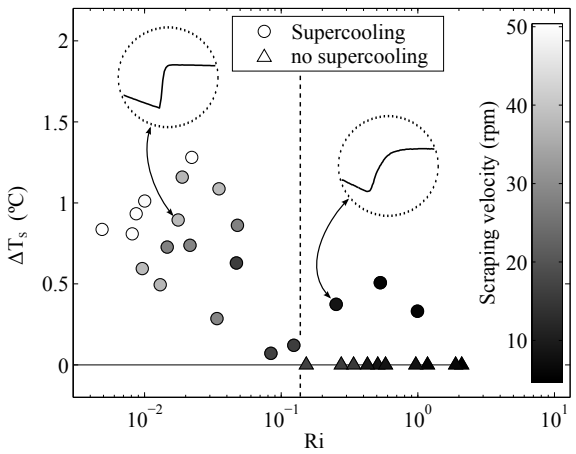

Figure 6. Supercooling amplitude (ΔT_S) vs. Richardson number.

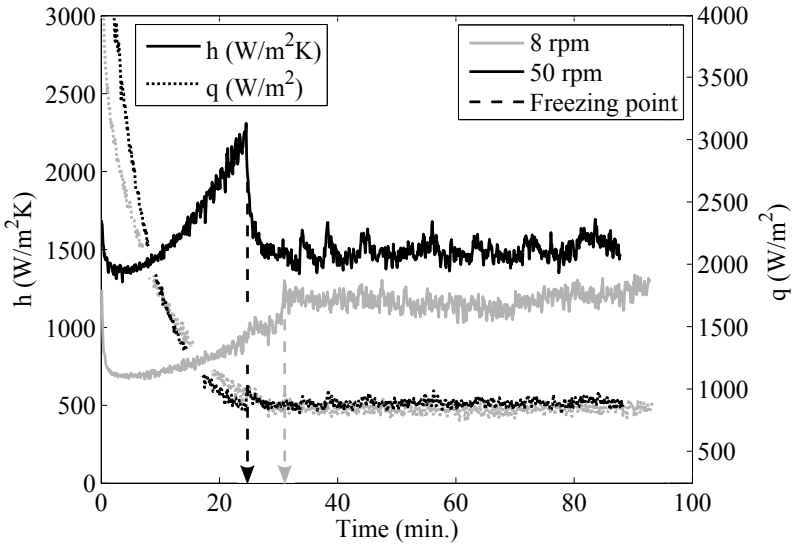

Figure 7. Heat flux q (W/m^2) and heat transfer coefficient h (W/m^{2}K evolution along time for 8 and 50 rpm rotating velocity tests)

As it was expected, ΔT_S decreases as Ri increases, finding that no supercooling is detected after $Ri \approx 0.1$. For those cases natural convection effects become important and the nucleation starts in the freezing wall, where an ice layer of thickness $\leq \delta$ appears. Nucleation starts then in the bottom of the volume and moves up gradually so that no supercooling is detected by the immersed probes located at H/2. However, some points with $Ri > 0.1$ showed to have supercooling. This can be explained considering that those points correspond to the lowest values of $\overline{\Delta T}_C$. As a consequence, in spite of the thermal stratification effect, the temperature of the bottom wall was higher than the freezing temperature of the NaCl brine and thus, the nucleation could not start and no ice layer was developed. Even so, the presence of the thermal stratification is noticeable if the two temperatures are compared along time. The supercooling on the left ($Ri < 0.1$) presents a sharp change on the temperature and almost an instantaneous increment. The supercooling on the right ($Ri > 0.1$) presents a smoother change with a slower temperature increment.

Figure 7 plots the instantaneous heat flux q together with the instantaneous heat transfer coefficient h, calculated according to Eq. 5 for two different tests at 8 and 50 rpm rotating velocities with same $\overline{\Delta T}_C$. The 8 rpm case shows a h value that constantly increases until the nucleation point is reached and the freezing process starts. During the initial period, the heat is accumulated in form of sensible heat until the nucleation starts and it is transformed into latent heat, showing a uniform heat transfer coefficient during all the process. On the other hand, the heat transfer coefficient for the 50 rpm case decreases once the nucleation starts. In this case the negative effect of the heat resistance created by the ice layer over the freezing surface is then higher than the beneficial effect of the ice formation and its high latent heat of fusion.

To provide a better idea of the effect on the heat transfer, Fig. 8 shows the values of the averaged heat transfer coefficient during all the freezing period $\overline{h}$ versus the averaged difference of temperatures $\overline{\Delta T}_C$. The maximum values of $\overline{h}$ are grouped around $\overline{\Delta T}_C$ =2.5 °C, whereas the rotating velocity (colour mark) seems not to have a clear effect. Up to $\overline{\Delta T}_C \approx 3$ °C the values of $\overline{h}$ tend to an asymptote of $\overline{h} \approx 1000$ W/m^{2}K, regardless of their rotational velocity. The strong ice layer formed over the freezing surface at large $\overline{\Delta T}_C$ values could be the responsible of this stabilization.

To highlight the effect of thermal stratification, a new $\overline{Ri}$ number was computed following Eq. 8 and replacing $\overline{T}_f - \overline{T}_w$ by $\overline{\overline{T}_f - \overline{T}_w}$, averaged in all the freezing period. Again the cases where supercooling was detected appear for $\overline{Ri}$ >0.1 1, with the exception of the cases with a low $\overline{\Delta T}_C$. If a constant rotating velocity is considered, for instance 50 rpm (white marks), it decreases suddenly as long as $\overline{Ri}$ increases, with a $\overline{h}$ decrement of around 400 W/m^{2}K. This behaviour can be observed for different scraping velocities but it becomes less important as $\overline{Ri}$ increases. On the other hand, if a constant $\overline{Ri}$ value is considered, for example $\overline{Ri} \approx 10^{-2}$, an increment in the rotating speed produces lower $\overline{h}$ values. The last means that the increment of $\overline{\Delta T}_C$ has a higher beneficial effect on $\overline{h}$ than the increment on the rotating speed (under equal natural-forced convection ratios). For $\overline{Ri}$ >0.1 the values of $\overline{h}$ are almost uniform and equal to 1000 W/m^{2}K. The effect of the thermal stratification plays a negative role in the heat transfer, hindering the mixing phenomenon. Moreover, strong ice layers are formed over the freezing surface, increasing the heat transfer resistance.

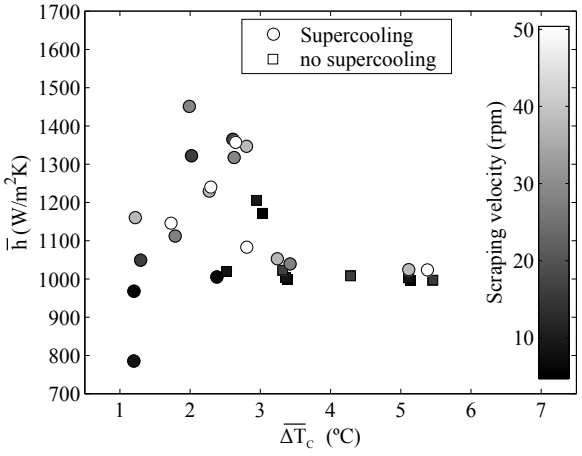

Figure 8. Averaged heat transfer coefficient $\overline{h}$ vs. coolant temperature difference $\overline{\Delta T}_C$.

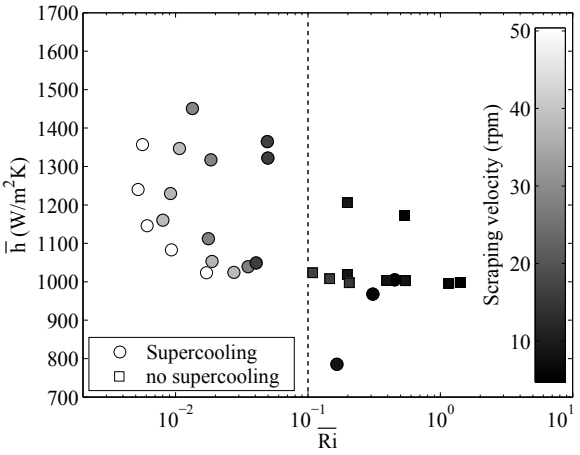

Figure 9. Averaged heat transfer coefficient $\overline{h}$ vs. averaged Richardson number $\overline{Ri}$.

As a conclusion, it can be said that the optimal parameters for the ice slurry production for the tested brine (5% of NaCl solution in water) are $\overline{\Delta T}_C \geq 2.5$ °C, where maximum $\overline{\zeta}$ values are found, keeping $\overline{Ri}$ <0.1.

5. Conclusions

- An innovative-scraped surface plate heat exchanger (SSPHE) was designed for freezing NaCl aqueous solutions. It consists of a tank with a total heat transfer area of 10m^{2}m^{-3} crystallizer volume where four rotating PEEK blades, driven by a vertical shaft connected to an electrical motor, scrape continuously the surface. The heat transfer surface is cooled underneath by a flow of calcium chloride solution in water, subsequently cooled by the expansion of a flow of R507 refrigerant in a compact evaporator.
- The heat transfer in the SSPHE was experimentally studied when used for freezing NaCl aqueous solutions in 5 wt.% concentration for different rotating speeds of the scraper blades (5-50 rpm) and different coolant temperatures ($1 \leq \overline{\Delta T}_C \leq 6$). The heat transfer coefficient values where computed from wall temperature measurements (embedded thermocouples) and fluid temperature measurements (immersed PT100 probes). The observed freezing point temperature was in good agreement with the predictions from the available correlations [10].

- The averaged freezing speed $\overline{\zeta}$ was found to increase linearly with $\overline{\Delta T}_C$ until $\overline{\Delta T}_C \approx 3.5$ °C, where it stabilizes around 0.014 °C/min. Supercooling phenomena showed to be dependent on the Ri number, being detected only when $Ri < 0.1$ and increasing its amplitude as Ri decreases. $Ri > 0.1$ values lead to lower $\overline{\zeta}$ due to the strong thermal stratification and to the formation of an ice layer over the freezing surface. The effect of the scraping velocity showed a low influence.
- Maximum heat transfer coefficient values for the SSPHE of 1400 W/m^{2}K were found for $\overline{\Delta T}_C \geq 2.5$ °C and $\overline{Ri} < 0.1$. $\overline{h}$ values for equal rotating speeds showed to be very sensible to Ri variations, decreasing rapidly as Ri increases. On the other hand constant Ri values showed a decrease on $\overline{h}$ for rotating speed increments, concluding that the effect of $\overline{\Delta T}_C$ is much higher than the effect of the scraping velocity.

References

[1] Rao, Chetan S., Hartel, Richard W., 2006. Critical Reviews in Food Science and Nutrition

[2] Vaessen, R.J.C., Seckler, M.M., and Witkamp, G.J., 2003. Heat Mass Transfer, Vol. 47, pp. 717-728

[3] Qin, F.G.F., Chen, X.D., and Russell, A.B., 2003. AIChE Journal, Vol. 49, pp. 1947- 1955.

[4] Pascual, M. Ravelet, F. Delfos, R. Derksen, J.J. Witkamp, G.J., 2009. Chemical Engineering Science, Vol. 64, pp. 2127-2135

[5] Melinder, A., 1997. *Thermophysical properties of liquid secondary refrigerants*, International Institute of Refrigeration

[6] Kane, S. G., 1971. *Secondary nucleation of ice in a stirred batch crystallizer*, SC.D. Thesis, Mass. Inst. Technol., Cambridge.

[7] Kane, S. G., Evans, T. W., Brian, P. L. T., Sarofem, A. F., 1974. *Determination of the kinetics of secondary nucleation in batch crystallizers*, AIChE Journal, Vol. 20, Num. 5, pp. 855-862

[8] Omram, A. M., King, C. J., 1974. *Kinetics of ice crystallization in sugar solution and fruit juices*, AIChE Journal, Vol. 20, Num. 4, pp. 795-802

[9] Stocking, J. H., King, C. J., 1976. *Secondary nucleation of ice in sugar solutions and fruit juices*, AIChE Journal, Vol. 22, Num. 1 pp. 131-140.

[10] Melinder, A., 2007. *Thermophysical Properties of Aqueous Solutions Used as Secondary Working Fluids*, Thesis, Royal Institute of Technology, KTH, Sweden

[11] Qin, F.G.F., Zhao, J. C., Russell, A.B., Chen, X. D., Chen, J. J., Robertson, L., 2003. *Simulation and experiment of the unsteady heat transport in the onset time of nucleation and crystallization of ice form subcooled solution*, International Journal of Heat and Mass Transfer, Vol. 46, pp. 3221-3231